Generation Expansion Planning Considering Discrete Storage Model and Renewable Energy Uncertainty: A Bi-Interval Optimization Approach

Siyuan Wang, Guangchao Geng, *Senior Member, IEEE*, Quanyuan Jiang, *Senior Member, IEEE*, and Rui Bo, *Senior Member, IEEE*

***Abstract*—Both discrete storage model (DSM) and continuous storage model (CSM) have been used in the power system planning literature. In this work, we conduct a sizing-error analysis for the use of CSM in generation expansion planning (GEP), which shows more reasonable storage sizing decisions are offered by the DSM in comparison to the CSM. However, when the DSM is considered in the context of interval optimization, the discrete status variables in mutually exclusive constraints and the strong temporal coupling in state-of-charge (SOC) constraints create significant challenges. To tackle this, a tailored interval optimization approach is proposed to consider both DSM and renewable energy uncertainty in GEP. Our approach is proved to cover all worst cases in a given uncertainty set, meanwhile running in an iteration-free manner. Moreover, to reduce the conservativeness of investment decisions, a bi-interval policy is designed to achieve a better trade-off between investment cost and system security.**

***Index Terms*—energy storage, generation expansion planning, renewable energy uncertainty, interval optimization.**

NOMENCLATURE

Indices and Sets

i, s, t	Index of devices in the power system, scenarios, and time periods
$\Omega_{\rm g}, \Omega_{\rm ng}$	Set of existing and candidate generators
$\Omega_{\rm w}, \Omega_{\rm nw}$	Set of existing and candidate renewable energy sources
$\Omega_{\rm nes}$	Set of candidate energy storage
$\mathcal{S}, \mathcal{T}$	Set of scenarios and time periods

Parameters

N_s, N_t	Number of scenarios and time periods
τ_s	Number of days represented by the base case scenario s in a year
X_i	Annualized investment cost of generator i
α_i, β_i	Annualized investment cost per unit power capacity of renewable energy source or storage i, and annualized investment cost per unit energy capacity of storage i
$C^{\rm gen}_{i,s,t}$	Operation cost of generator i in time period t of scenario s
$C^{\rm ch}_{i,s,t}, C^{\rm dc}_{i,s,t}$	Charging and discharging operation cost of storage i in time period t of scenario s
$\hat{P}_i$	Power capacity of existing renewable energy source i
$wc_{i,s,t}$	Normalized available power for existing and candidate renewable energy source i in time period t of scenario s
$d_{s,t}$	System load in time period t of scenario s
φ	Maximum ratio for load shedding
$n_i^{\max}$	Maximum number of candidate generator i
CE_i	Carbon emission per unit of electricity for generator i
CET	Annual total carbon emission limit
CF_i	Maximum capacity factor for generator i
$\hat{n}_i$	Number of existing generators i
$\overline{P}_i, \underline{P}_i$	Maximum and minimum power output for generator i
RU_i, RD_i	Upward and downward ramp rate limits for generator i
$P_i^{\max}, E_i^{\max}$	Maximum power capacity of candidate energy storage or candidate renewable energy source i, and maximum energy capacity of candidate energy storage i
$\delta_i, \eta_i^{\rm ch}, \eta_i^{\rm dc}$	Self-discharge rate, charging efficiency, and discharging efficiency for energy storage i
$\overline{\gamma}_{i,s,t}, \underline{\gamma}_{i,s,t}$, $\gamma_{i,s,0}$	Normalized upper bound, lower bound, and initial state of charge levels for energy storage i in time period t of scenario s

Decision Variables

n_i	Integer decision variable for the number of candidate generator i to build
P_i, E_i	Power capacity of candidate renewable energy source or energy storage i, and energy capacity of energy storage i
$d^{\rm s}_{s,t}$, $w^{\rm c}_{s,t}$	Load shedding and renewable curtailment in

Manuscript received January 20, 2022; revised March 20, 2022; accepted May 16, 2022. The work of G. Geng and Q. Jiang was supported by the Fundamental Research Funds for the Central Universities under Grant 226-2022-00164. An earlier version of this work is shown in S. Wang's Ph.D. dissertation [1]. Paper no. TII-22-0321. *(Corresponding author: Guangchao Geng.)*

S. Wang was with the College of Electrical Engineering, Zhejiang University, Hangzhou 310027, China. He is now with the Whiting School of Engineering, Johns Hopkins University, Baltimore, MD 21218, USA (e-mail: sywang@zju.edu.cn; siyuanwang@jhu.edu).

G. Geng and Q. Jiang are with the College of Electrical Engineering, Zhejiang University, Hangzhou 310027, China (e-mail: ggc@zju.edu.cn; jqy@zju.edu.cn).

R. Bo is with the Department of Electrical and Computer Engineering, Missouri University of Science and Technology, Rolla, MO 65409, USA (e-mail: rbo@mst.edu).

This article has been accepted for publication in IEEE Transactions on Industrial Informatics.

	time period t of scenario s
$p_{i,s,t}$	Injection power from generator or energy storage i in time period t of scenario s
$u^{\text{ch}}_{i,s,t}, u^{\text{dc}}_{i,s,t}$	Binary charging and discharging status variables for energy storage i in time period t of scenario s
$p^{\text{ch}}_{i,s,t}, p^{\text{dc}}_{i,s,t}$	Charging and discharging power for energy storage i in time period t of scenario s
$e_{i,s,t}$	State of charge for energy storage i in time period t of scenario s

I. Introduction

THE fluctuating and uncertain nature of renewable energy is recognized as a significant challenge to maintain power system security. Energy storage technology is a promising option to address this challenge. Therefore, the inclusion of storage options in power system planning has raised increasing attention recently.

Generation expansion planning (GEP) has been broadly investigated to offer optimal generation mixes [2]. Recent works have incorporated energy storage candidates into GEP formulations to address the intermittency of renewable energy [3]. In the literature, both *continuous storage model* (CSM) [4]–[7] and *discrete storage model* (DSM) [8]–[11] are incorporated into GEP and related power system planning problems. Binary variables are used in the DSM to represent exclusive charging and discharging statuses of storage, while they are eliminated in the CSM[1], which can be viewed as a relaxation of the DSM. For a specific economic dispatch problem, the relaxed CSM is analytically proved to be exact under certain sufficient conditions [12]. Numerical counter examples for transmission planning and unit commitment are shown in [13]. A similar observation was earlier presented in the first author's dissertation [1] in the context of GEP, which was conducted independently of the work in [13]. In our analysis in Section III and corresponding numerical verification, we show how the relaxed CSM is generally inexact in GEP in terms of storage sizing decisions. We also find, due to the inherent energy conversion losses modeled in the state-of-charge (SOC) constraints, allowing simultaneously charging and discharging in the CSM may lead to lower energy capacities of storage and therefore lower investment cost, which is considered a main cause of the aforementioned storage sizing error.

To address renewable energy uncertainty, the two-stage optimization framework, wherein planning and operation decisions are made in the first and second stages, respectively, has been used with stochastic programming (SP), robust optimization (RO), and interval optimization (IO). Incorporating the DSM in the second stage can bring significant challenges to such two-stage problems, as traditional separation algorithms rely on an assumption of convex recourse. As summarized in Table I, the CSM is widely used in SP [4]–[6] and RO [7]. Furthermore, binary status variables in the DSM are decided in the planning stage of RO to guarantee linear program (LP) recourse [9], [10]. Only a few iterative approaches[2] have been proposed for two-stage optimization with DSM in the operation stage, such as SP in [8] and RO in [11]. However, complicated problem formulation and iterative solution approaches may not be computationally reliable for practical applications. IO is an appealing iteration-free approach, but addressing the DSM in the operation stage is challenging.

TABLE I
Taxonomy of Works on Power System Planning with Storage

planning works	DSM in the operation stage	uncertainty consideration	iteration-free approach
[4] [5]	no (CSM)	yes (SP)	no
[6]	no (CSM)	yes (SP)	yes
[8]	yes	yes (SP)	no
[7]	no (CSM)	yes (RO,SP)	no
[9] [10]	no (DSM with binaries in the planning stage)	yes (RO)	no
[11]	yes	yes (RO)	no
this work	yes	yes (IO)	yes

Early theories on IO [14] guarantee the validity of this approach on a time-decoupled basis. In [15], [16], time-coupled ramp constraints of generators are further addressed. When the DSM is incorporated in GEP in an IO context, two main challenges are encountered: 1) binary status variables in the DSM dispute the validity of the theory in [14], which assumes LP recourse; 2) SOC constraints pose stronger time-coupling, which is also challenging to address. To tackle these challenges, a tailored IO approach is proposed for GEP with DSM in an iteration-free manner. We also show that our approach can cover all the worst cases in a given uncertainty set. It is worth mentioning that modeling ambient temperature impacts [17] and state of health (SOH) [18], [19] for battery storage would further complicate the planning decision making under uncertainty, which could be a good research topic to explore, but is beyond the scope of this work.

In comparison to SO, both IO and RO approaches are believed to be more secure, but more conservative [16]. Although the conservativeness can be adjusted by tuning uncertainty set parameters, an appropriate trade-off between system security performance and investment cost is usually difficult to achieve. The approach would be over-conservative when the uncertainty set is too large, while insecure when the uncertainty set is too small. To this end, a bi-interval policy is proposed in this work to address the conservativeness issue by applying distinct load shedding and renewable curtailment limits to different confidence intervals. The proposed approach can avoid paying high investment costs for rarely happened cases.

The main contributions of this work are,

1) We analyze and numerically verify how the relaxed CSM is generally inexact in terms of storage sizing in GEP. We find

[1]Note complementarity constraints in (9), which will be shown in section III, can be added to avoid simultaneously charging and discharging in the CSM. However, this results in a mixed-integer non-linear model for GEP. To render the problem tractable, the CSMs in the planning literature usually do not contain complementarity constraints in (9). Thus, we refer CSM to the model without complementarity constraints, as shown later in (8) and (6d)-(6h).

[2]SP with DSM in the operation stage doesn't have to be solved in an iterative manner [6]. However, as SP heavily relies on the quality and quantity of scenarios, with massive scenarios considered, iterative approaches are usually needed to address scalability issues.

allowing simultaneously charging and discharging in the CSM can lead to lower energy capacities of storage and therefore lower investment costs, due to the inherent energy conversion losses modeled in the SOC constraints.

2) A tailored IO approach is proposed to address binary variables and temporal SOC constraints when the DSM is used in the operation stage of GEP. Our approach is shown to cover all worst cases in a given uncertainty set, meanwhile addressing renewable energy uncertainty in an iteration-free manner. A bi-interval policy is further designed to reduce conservativeness.

3) Our approach is tested on Gansu power grid case with meteorological data for renewable energy resources. Storage is shown to be an essential option for a low-carbon power system. The investment cost per unit of energy capacity for battery storage has a significant impact on the overall cost.

II. Problem Formulation

This section describes our problem formulation, however, we leave the details of IO constraints in section IV for the convenience of demonstration.

A. Objective Function

The objective function is expressed in (1), which is the sum of annualized investment cost (*term a* for generators, *term b* for energy storage, and *term c* for renewable energy sources) and system operation cost (*term d* for generators, and *term e* for energy storage).

$$\min \quad \underbrace{\sum\nolimits_{i\in\Omega_{\mathrm{ng}}} X_i n_i}_{term\ a} + \underbrace{\sum\nolimits_{i\in\Omega_{\mathrm{nes}}} (\alpha_i P_i + \beta_i E_i)}_{term\ b} + \underbrace{\sum\nolimits_{i\in\Omega_{\mathrm{nw}}} \alpha_i P_i}_{term\ c} + \sum\nolimits_{s\in\mathcal{S}} \sum\nolimits_{t\in\mathcal{T}} \tau_s \cdot \Big[\underbrace{\sum\nolimits_{i\in\Omega_{\mathrm{g}}\cup\Omega_{\mathrm{ng}}} C^{\mathrm{gen}}_{i,s,t} p_{i,s,t}}_{term\ d} + \underbrace{\sum\nolimits_{\Omega_{\mathrm{nes}}} \left(C^{\mathrm{dc}}_{i,s,t} p^{\mathrm{dc}}_{i,s,t} + C^{\mathrm{ch}}_{i,s,t} p^{\mathrm{ch}}_{i,s,t}\right)}_{term\ e} \Big] \tag{1}$$

B. Constraints in Planning Scale

1) Generator Constraints: The number of candidate generators to build is limited in (2a). The annual carbon emission produced by the system is constrained in (2b) with a one-hour interval assumption. Maximum capacity factor constraints for existing and candidate generators are presented in (2c) and (2d), respectively.

$$0 \le n_i \le n_i^{\max} \quad \forall i \in \Omega_{\mathrm{ng}} \tag{2a}$$

$$\sum\nolimits_{i\in\Omega_{\mathrm{g}}\cup\Omega_{\mathrm{ng}}} \sum\nolimits_{s\in\mathcal{S}} \sum\nolimits_{t\in\mathcal{T}} \tau_s \cdot CE_i \cdot p_{i,s,t} \le CET \tag{2b}$$

$$\sum\nolimits_{s\in\mathcal{S}} \sum\nolimits_{t\in\mathcal{T}} \tau_s \cdot p_{i,s,t} \le 8760 \cdot CF_i \cdot \overline{P}_i \cdot \hat{n}_i \ \forall i \in \Omega_{\mathrm{g}} \tag{2c}$$

$$\sum\nolimits_{s\in\mathcal{S}} \sum\nolimits_{t\in\mathcal{T}} \tau_s \cdot p_{i,s,t} \le 8760 \cdot CF_i \cdot \overline{P}_i \cdot n_i \ \forall i \in \Omega_{\mathrm{ng}} \tag{2d}$$

2) Renewable Energy Source and Energy Storage Constraints: The power capacities of renewable energy sources are limited by resource potential, as shown in (3a). For specific types of energy storage, such as pumped storage, the power and energy capacities are also limited in (3b). As (6a)-(6b) and (6g)-(6h) ensure positive values of P_i and E_i, lower bounds are not modeled in (3b).

$$0 \le P_i \le P_i^{\max} \quad \forall i \in \Omega_{\mathrm{nw}} \tag{3a}$$

$$P_i \le P_i^{\max},\ E_i \le E_i^{\max} \quad \forall i \in \Omega_{\mathrm{nes}} \tag{3b}$$

C. Constraints in Operation Scale

1) System Constraints: The system power balance constraint is described in (4) for each time period.

$$\sum\nolimits_{i\in\Omega_{\mathrm{g}}\cup\Omega_{\mathrm{ng}}} p_{i,s,t} + \sum\nolimits_{i\in\Omega_{\mathrm{nes}}} p_{i,s,t} + \sum\nolimits_{i\in\Omega_{\mathrm{w}}} wc_{i,s,t} \cdot \hat{P}_i + \sum\nolimits_{i\in\Omega_{\mathrm{nw}}} wc_{i,s,t} \cdot P_i = d_{s,t} \quad \forall s,t \tag{4}$$

2) Generator Constraints: Power output of existing and candidate generators are bounded in (5a) and (5c), respectively. Ramp rate constraints are expressed in (5b) and (5d). Tie lines can be treated as special existing generators, as modeled in (5c), with $\underline{P}_i$ and $\overline{P}_i$ defined as lower and upper bounds for net import flows, respectively.

$$\underline{P}_i \cdot \hat{n}_i \le p_{i,s,t} \le \overline{P}_i \cdot \hat{n}_i \quad \forall i \in \Omega_{\mathrm{g}}, s, t \tag{5a}$$

$$-RD_i \cdot \hat{n}_i \le p_{i,s,t+1} - p_{i,s,t} \le RU_i \cdot \hat{n}_i \quad \forall i \in \Omega_{\mathrm{g}}, s, t \in \mathcal{T} \setminus \{N_t\} \tag{5b}$$

$$\underline{P}_i \cdot n_i \le p_{i,s,t} \le \overline{P}_i \cdot n_i \quad \forall i \in \Omega_{\mathrm{ng}}, s, t \tag{5c}$$

$$-RD_i \cdot n_i \le p_{i,s,t+1} - p_{i,s,t} \le RU_i \cdot n_i \quad \forall i \in \Omega_{\mathrm{ng}}, s, t \in \mathcal{T} \setminus \{N_t\} \tag{5d}$$

3) Energy Storage Constraints: Discharging and charging power levels are bounded in (6a) and (6b), respectively. A mutually exclusive relation for charging and discharging statuses is established with binary variables in (6c). With this constraint, simultaneous charging and discharging, which would not happen in physical systems, can be avoided. The net power injections from energy storage are expressed in (6d). SOC is calculated in (6e) and bounded in (6f)-(6h).

$$0 \le p^{\mathrm{dc}}_{i,s,t} \le P_i^{\max} u^{\mathrm{dc}}_{i,s,t},\ p^{\mathrm{dc}}_{i,s,t} \le P_i \quad \forall i \in \Omega_{\mathrm{nes}}, s, t \tag{6a}$$

$$0 \le p^{\mathrm{ch}}_{i,s,t} \le P_i^{\max} u^{\mathrm{ch}}_{i,s,t},\ p^{\mathrm{ch}}_{i,s,t} \le P_i \quad \forall i \in \Omega_{\mathrm{nes}}, s, t \tag{6b}$$

$$u^{\mathrm{ch}}_{i,s,t} + u^{\mathrm{dc}}_{i,s,t} \le 1 \quad \forall i \in \Omega_{\mathrm{nes}}, s, t \tag{6c}$$

$$p_{i,s,t} = p^{\mathrm{dc}}_{i,s,t} - p^{\mathrm{ch}}_{i,s,t} \quad \forall i \in\ \Omega_{\mathrm{nes}}, s, t \tag{6d}$$

$$e_{i,s,t} = (1-\delta_i) \cdot e_{i,s,t-1} + \eta^{\mathrm{ch}}_i \cdot p^{\mathrm{ch}}_{i,s,t} - 1/\eta^{\mathrm{dc}}_i \cdot p^{\mathrm{dc}}_{i,s,t} \quad \forall i \in \Omega_{\mathrm{nes}}, s, t \tag{6e}$$

$$e_{i,s,0} = \gamma_{i,s,0} E_i \quad \forall i \in \Omega_{\mathrm{nes}}, s \tag{6f}$$

$$\underline{\gamma}_{i,s,t} E_i \le e_{i,s,t} \le \overline{\gamma}_{i,s,t} E_i \quad \forall i \in \Omega_{\mathrm{nes}}, s, t \in \mathcal{T} \setminus \{N_t\} \tag{6g}$$

$$\underline{\gamma}_{i,s,N_t} E_i \le e_{i,s,N_t} \le \overline{\gamma}_{i,s,N_t} E_i \quad \forall i \in \Omega_{\mathrm{nes}}, s \tag{6h}$$

Note (6a)-(6h) formulate the DSM. Further analysis of using DSM and CSM in GEP will be presented in section III.

4) Interval Optimization Constraints: To ensure the system operational security under renewable energy uncertainty, an IO approach is proposed with a bi-interval policy. The IO constraints are abstractly expressed in (7), and will be described in section IV in detail.

$$\mathbf{IOCons}\left(\boldsymbol{n}, \boldsymbol{P}, \boldsymbol{E}\right) \leq \mathbf{0} \tag{7}$$

where, $\boldsymbol{n} = \{n_i : \forall i \in \Omega_{\text{ng}}\}$, $\boldsymbol{P} = \{P_i : \forall i \in \Omega_{\text{nw}} \cup \Omega_{\text{nes}}\}$, and $\boldsymbol{E} = \{E_i : \forall i \in \Omega_{\text{nes}}\}$.

III. Continuous Storage Model v.s. Discrete Storage Model: An Error Analysis

As summarized in the introductory section, various power system planning works use the CSM, in which the mutually exclusive constraints in (6c) or the complementarity constraints (i.e., $p^{\text{dc}}_{i,s,t} \cdot p^{\text{ch}}_{i,s,t} = 0,\ \forall i \in \Omega_{\text{nes}}, s, t$) are eliminated. The CSM simplifies the uncertainty handling process, especially for IO and RO, as the sub-problem in the operation stage is an LP. Essentially, the CSM is a relaxation of the DSM, i.e., the constraints to avoid simultaneous charging and discharging are relaxed. We observed this relaxation is generally inexact for GEP and may lead to significant errors in storage capacities.

In this work, the DSM is formulated in (6a)-(6h) as shown in section II, while the CSM is formulated in (8) and (6d)-(6h).

$$0 \leq p^{\text{dc}}_{i,s,t} \leq P_i,\ 0 \leq p^{\text{ch}}_{i,s,t} \leq P_i \quad \forall i \in \Omega_{\text{nes}}, s, t \tag{8}$$

Suppose the optimal solution from a GEP problem with DSM be $\tilde{p}^{\text{dc}}_{i,s,t}$ and $\tilde{p}^{\text{ch}}_{i,s,t}$, then we have (9).

$$\tilde{p}^{\text{dc}}_{i,s,t} \cdot \tilde{p}^{\text{ch}}_{i,s,t} = 0 \quad \forall i \in \Omega_{\text{nes}}, s, t \tag{9}$$

Now we show the reason of deviating from the solution $\tilde{p}^{\text{dc}}_{i,s,t}$ and $\tilde{p}^{\text{ch}}_{i,s,t}$ when the CSM is used. As the charging and discharging power usually do not reach their limits in all the time periods, this leaves spaces for them to simultaneously increase by $\Delta p_{i,s,t}$ in the CSM while keeping the network injection power unchanged. Note the constraints (6e)-(6h) are equivalent to (10), in which the variables $e_{i,s,t}$ are canceled for convenience.

$$\begin{aligned}&\gamma_{i,s,t} E_i \leq (1-\delta_i)^t \gamma_{i,s,0} E_i + \sum\nolimits_{t'=1}^{t} (1-\delta_i)^{t-t'} \cdot \\ &\left(\eta^{\text{ch}}_i \cdot p^{\text{ch}}_{i,s,t'} - 1/\eta \cdot p^{\text{dc}}_{i,s,t'}\right) \leq \overline{\gamma}_{i,s,t} E_i \quad \forall i \in \Omega_{\text{nes}}, s, t\end{aligned} \tag{10}$$

Applying the updated discharging and charging power of energy storage (i.e., $\tilde{p}^{\text{dc}}_{i,s,t} + \Delta p_{i,s,t}$ and $\tilde{p}^{\text{ch}}_{i,s,t} + \Delta p_{i,s,t}$, respectively) to (10), we have (11).

$$\begin{aligned}&\sum\nolimits_{t'=1}^{t} (1-\delta_i)^{t-t'} \left(\eta^{\text{ch}}_i \cdot \tilde{p}^{\text{ch}}_{i,s,t'} - 1/\eta^{\text{dc}}_i \cdot \tilde{p}^{\text{dc}}_{i,s,t'} + \right. \\ &\left. \left(\eta^{\text{ch}}_i - 1/\eta^{\text{dc}}_i\right) \Delta p_{i,s,t'}\right) \leq \left(\overline{\gamma}_{i,s,t} - (1-\delta_i)^t \cdot \gamma_{i,s,0}\right) E_i \\ &\qquad \forall i \in \Omega_{\text{nes}}, s, t\end{aligned} \tag{11}$$

It is worth mentioning, $\eta^{\text{ch}}_i - 1/\eta^{\text{dc}}_i$ is negative as both η^{ch}_i and η^{dc}_i are in the range of $(0, 1)$. Simultaneously increasing both discharging and charging power by $\Delta p_{i,s,t}$ can result in a decrease in the LHS of (11). This can potentially reduce the optimal energy capacity E_i in the RHS of (11), which is driven by the benefit of decreasing investment cost term $\beta_i \cdot E_i$ for candidate storage in the optimization model.

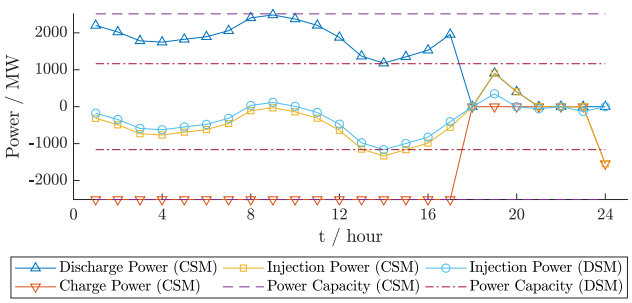

Fig. 1. Comparison of operation decisions from CSM and DSM.

Note such benefit could also exist even when both discharging and charging power related terms in the objective function are positive. In this case, although operation cost of storage increases by $(C^{\text{dc}}_{i,s,t} + C^{\text{ch}}_{i,s,t}) \cdot \Delta p_{i,s,t}$ in time period t, the increase of the operation cost in some time periods usually cannot match the decrease in the investment cost.

We also observe sometimes the increase of power capacity P_i may help reducing energy capacity E_i. Given a scenario s^* and a time period t^* for which (11) is bind, we have (12) to analyze how simultaneously increasing both discharging and charging power by $\Delta p_{i,s,t}$ can reduce the size of energy capacity E_i. In (12), an estimation of energy capacity E_i reduction is denoted as ΔE_i.

$$\Delta E_i \approx \frac{\sum_{t'=1}^{t^*} (1-\delta_i)^{t-t'} \cdot \left(1/\eta^{\text{dc}}_i - \eta^{\text{ch}}_i\right) \cdot \Delta p_{i,s^*,t'}}{\overline{\gamma}_{i,s^*,t^*} - (1-\delta_i)^{t^*} \cdot \gamma_{i,s^*,0}} \tag{12}$$

Meanwhile, the increment $\Delta p_{i,s^*,t'}$ is limited by the power capacity P_i, as shown in (13).

$$\Delta p_{i,s^*,t'} \leq \min\left\{P_i - \tilde{p}^{\text{dc}}_{i,s^*,t'},\ P_i - \tilde{p}^{\text{ch}}_{i,s^*,t'}\right\} \ \forall t' \leq t^* \tag{13}$$

If the investment cost per unit of power capacity α_i for energy storage is not far greater than its investment cost per unit of energy capacity β_i, the power capacity P_i may also have potentials to increase. This would result in the increase of $\Delta p_{i,s^*,t'}$, and thus the increase of ΔE_i. As ΔE_i is expressed in an integral form of $\Delta p_{i,s^*,t'}$ for $t' \leq t^*$ in (12), the cumulative effect may further benefit the aforementioned simultaneously charging and discharging behavior.

Fig. 1 shows an example of storage operations from GEP problems with CSM and DSM for the modified IEEE reliability test system in section V. As indicated, values of network injection power from both CSM and DSM are very close, but simultaneous charging and discharging behavior exists in the CSM case. This behavior takes advantage of negative $\eta^{\text{ch}}_i - 1/\eta^{\text{dc}}_i$ value to decrease the LHS of (11), and thus the energy capacity E_i. This matches our previous analysis.

IV. Interval Optimization Approach

In this section, our proposed constraints for IO are presented first. They are then shown to cover all worst cases in a given uncertainty set. A bi-interval policy is introduced to reduce conservativeness.

A. Interval Optimization Constraints

As stronger time-coupled constraints and binary status variables are incorporated in the operation stage, we can no longer directly use the Theorem 6 in [14], which guarantees the worst case would only occur in two possible uncertainty realizations under pure LP and time decoupled assumptions. In light of the method used in [14], we keep two cases in the constraints. In one case, renewable generation levels reach corresponding upper bounds simultaneously for all time periods. The related variables are marked with superscript U. In another case, renewable generation levels reach corresponding lower bounds simultaneously, and the related variables are marked with superscript L. Corresponding to constraints in (4)-(6), the operation constraints for the aforementioned two cases are shown in (14a)-(14c), (14e)-(14f), (14i)-(14l), and (14n)-(14q). In this work, connection constraints between the two cases are proposed, as shown in (14d), (14g)-(14h), and (14m).

We find the proposed formulation can cover all the worst cases in the uncertainty set shown in (15), which will be formally described and proved in the subsection IV-B. Note a *brute force* formulation that includes all combinations of renewable generation levels for each time also has the same property. In comparison to such formulation, if the connection constraints (14d), (14g)-(14h), and (14m) are excluded, the proposed formulation is more loose, because it only considers two combinations. However, with these connection constraints, our formulation can cover all the worst cases in the given uncertainty set. The conservativeness of the proposed tighter formulation will be discussed in the case study. In comparison to RO, the advantage of the proposed approach lies in addressing uncertainty in an iteration-free manner.

$$\sum\nolimits_{i\in\Omega_{\rm g}\cup\Omega_{\rm ng}} p_{i,s,t}^{\rm U(L)} + \sum\nolimits_{i\in\Omega_{\rm nes}} p_{i,s,t}^{\rm U(L)} + \sum\nolimits_{i\in\Omega_{\rm w}} wc_{i,s,t}^{\rm U(L)}\cdot\hat{P}_i + \sum\nolimits_{i\in\Omega_{\rm nw}} wc_{i,s,t}^{\rm U(L)}\cdot P_i = d_{s,t}\quad\forall s,t \tag{14a}$$

$$\underline{P}_i\cdot\hat{n}_i \le p_{i,s,t}^{\rm U(L)} \le \overline{P}_i\cdot\hat{n}_i \quad \forall i\in\Omega_{\rm g}, s, t \tag{14b}$$

$$\underline{P}_i\cdot n_i \le p_{i,s,t}^{\rm U(L)} \le \overline{P}_i\cdot n_i \quad \forall i\in\Omega_{\rm ng}, s, t \tag{14c}$$

$$p_{i,s,t}^{\rm U} \le p_{i,s,t}^{\rm L} \quad \forall i\in\Omega_{\rm g}\cup\Omega_{\rm ng}, s, t \tag{14d}$$

$$-RD_i\cdot\hat{n}_i \le p_{i,s,t+1}^{\rm U(L)} - p_{i,s,t}^{\rm U(L)} \le RU_i\cdot\hat{n}_i \quad \forall i\in\Omega_{\rm g}, s, t\in\mathcal{T}\setminus\{N_t\} \tag{14e}$$

$$-RD_i\cdot n_i \le p_{i,s,t+1}^{\rm U(L)} - p_{i,s,t}^{\rm U(L)} \le RU_i\cdot n_i \quad \forall i\in\Omega_{\rm ng}, s, t\in\mathcal{T}\setminus\{N_t\} \tag{14f}$$

$$-RD_i\cdot\hat{n}_i \le p_{i,s,t+1}^{\rm U(L)} - p_{i,s,t}^{\rm L(U)} \le RU_i\cdot\hat{n}_i \quad \forall i\in\Omega_{\rm g}, s, t\in\mathcal{T}\setminus\{N_t\} \tag{14g}$$

$$-RD_i\cdot n_i \le p_{i,s,t+1}^{\rm U(L)} - p_{i,s,t}^{\rm L(U)} \le RU_i\cdot n_i \quad \forall i\in\Omega_{\rm ng}, s, t\in\mathcal{T}\setminus\{N_t\} \tag{14h}$$

$$0 \le p_{i,s,t}^{\rm dc\ U(L)} \le P_i^{\max} u_{i,s,t}^{\rm dc\ U(L)},\ p_{i,s,t}^{\rm dc\ U(L)} \le P_i \quad \forall i\in\Omega_{\rm nes}, s, t \tag{14i}$$

$$0 \le p_{i,s,t}^{\rm ch\ U(L)} \le P_i^{\max} u_{i,s,t}^{\rm ch\ U(L)},\ p_{i,s,t}^{\rm ch\ U(L)} \le P_i \quad \forall i\in\Omega_{\rm nes}, s, t \tag{14j}$$

$$u_{i,s,t}^{\rm ch\ U(L)} + u_{i,s,t}^{\rm dc\ U(L)} \le 1 \quad \forall i\in\Omega_{\rm nes}, s, t \tag{14k}$$

$$p_{i,s,t}^{\rm U(L)} = p_{i,s,t}^{\rm dc\ U(L)} - p_{i,s,t}^{\rm ch\ U(L)} \quad \forall i\in\Omega_{\rm nes}, s, t \tag{14l}$$

$$p_{i,s,t}^{\rm U} \le p_{i,s,t}^{\rm L} \quad \forall i\in\Omega_{\rm nes}, s, t \tag{14m}$$

$$e_{i,s,t}^{\rm U(L)} = (1-\delta_i)\cdot e_{i,s,t-1}^{\rm U(L)} + \eta_i^{\rm ch}\cdot p_{i,s,t}^{\rm ch\ U(L)} - 1/\eta_i^{\rm dc}\cdot p_{i,s,t}^{\rm dc\ U(L)} \quad \forall i\in\Omega_{\rm nes}, s, t \tag{14n}$$

$$e_{i,s,0}^{\rm U(L)} = \gamma_{i,s,0}E_i \quad \forall i\in\Omega_{\rm nes}, s \tag{14o}$$

$$\underline{\gamma}_{i,s,t}E_i \le e_{i,s,t}^{\rm U(L)} \le \overline{\gamma}_{i,s,t}E_i \quad \forall i\in\Omega_{\rm nes}, s, t\in\mathcal{T}\setminus\{N_t\} \tag{14p}$$

$$\underline{\gamma}_{i,s,N_t}^{\rm U(L)}E_i \le e_{i,s,N_t}^{\rm U(L)} \le \overline{\gamma}_{i,s,N_t}^{\rm U(L)}E_i \quad \forall i\in\Omega_{\rm nes}, s \tag{14q}$$

B. Property of the Formulation

Here we describe and prove a property of the proposed formulation, namely, covering all the worst cases in a predefined uncertainty set.

Property: Given fixed investment decision variables (i.e., n_i for generators, P_i for renewable energy sources, and P_i, E_i for energy storage), if there exists a feasible solution for constraints in (14), then there exists a feasible solution for operation constraints in (4)-(6) with any $wc \in U$. The uncertainty set U is defined in (15).

$$U = \left\{ \begin{array}{l} wc\in\mathbb{R}^{(|\Omega_{\rm w}|+|\Omega_{\rm nw}|)\cdot N_s\cdot N_t}: \\ wc_{i,s,t}\in\left[wc_{i,s,t}^{\rm L}, wc_{i,s,t}^{\rm U}\right],\ \forall i\in\Omega_{\rm w}\cup\Omega_{\rm nw}, s, t \end{array} \right\} \tag{15}$$

where, the vector $wc = \{wc_{i,s,t},\ \forall i\in\Omega_{\rm w}\cup\Omega_{\rm nw}, s, t\}$.

Proof. The proof of the property is organized in two parts. The first part provides the proof for any $wc\in U'$. As defined in (16), U' is a subset of U. The second part extends the uncertainty set from U' in the first part to U.

$$U' = \left\{ \begin{array}{l} wc\in\mathbb{R}^{(|\Omega_{\rm w}|+|\Omega_{\rm nw}|)\cdot N_s\cdot N_t}: \\ wc_{i,s,t} = wc_{i,s,t}^{\rm L} + \left(wc_{i,s,t}^{\rm U} - wc_{i,s,t}^{\rm L}\right)\cdot\sigma_{s,t} \\ \sigma_{s,t}\in\mathbb{B},\quad \forall i\in\Omega_{\rm w}\cup\Omega_{\rm nw}, s, t \end{array} \right\} \tag{16}$$

1) Proof for U': Given the condition that there exists a feasible solution for constraints in (14), we denote the solution as in (17)-(19). Note the SOC variables for energy storage, i.e., $e_{i,s,t}$, are not listed here, as they are dependent on charging and discharging power.

$$p_{i,s,t}^{\rm U(L)} = \tilde{p}_{i,s,t}^{\rm U(L)} \quad \forall i\in\Omega_{\rm g}\cup\Omega_{\rm ng}\cup\Omega_{\rm nes}, s, t \tag{17}$$

$$u_{i,s,t}^{\rm dc\ U(L)} = \tilde{u}_{i,s,t}^{\rm dc\ U(L)},\ u_{i,s,t}^{\rm ch\ U(L)} = \tilde{u}_{i,s,t}^{\rm ch\ U(L)} \quad \forall i\in\Omega_{\rm nes}, s, t \tag{18}$$

$$p_{i,s,t}^{\rm dc\ U(L)} = \tilde{p}_{i,s,t}^{\rm dc\ U(L)},\ p_{i,s,t}^{\rm ch\ U(L)} = \tilde{p}_{i,s,t}^{\rm ch\ U(L)} \quad \forall i\in\Omega_{\rm nes}, s, t \tag{19}$$

We assert a feasible solution of constraints (4)-(6) for any $wc\in U'$ can be represented in (20)-(22). To prove this, we need to check if all the constraints in (4)-(6) are satisfied.

$$p_{i,s,t} = \left\{ \begin{array}{l} \tilde{p}_{i,s,t}^{\rm U},\ \text{if } \sigma_{s,t}=1 \\ \tilde{p}_{i,s,t}^{\rm L},\ \text{if } \sigma_{s,t}=0 \end{array} \right. \quad \forall i\in\Omega_{\rm g}\cup\Omega_{\rm ng}\cup\Omega_{\rm nes}, s, t \tag{20}$$

$$p_{i,s,t}^{\rm dc} = \max\left\{p_{i,s,t}, 0\right\},\quad p_{i,s,t}^{\rm ch} = -\min\left\{p_{i,s,t}, 0\right\} \quad \forall i\in\Omega_{\rm nes}, s, t \tag{21}$$

$$u_{i,s,t}^{\rm dc} = \max\left\{\mathrm{sgn}(p_{i,s,t}), 0\right\},\quad u_{i,s,t}^{\rm ch} = 1 - u_{i,s,t}^{\rm dc} \quad \forall i\in\Omega_{\rm nes}, s, t \tag{22}$$

where, $\mathrm{sgn}(\cdot)$ is the sign function.

The non-temporal constraints in (4), (5a), (5c), and (6a)-(6d) are trivially satisfied for any $wc \in U'$ under the given solution. The temporal constraints, i.e., ramp constraints in (5b), (5d), and SOC constraints in (10) (i.e., as shown in section III, (6e)-(6h) can be reformulated as (10)) should be further examined.

As indicated in (20), the value of $p_{i,s,t}$ is either $\tilde{p}^{\mathrm{U}}_{i,s,t}$ or $\tilde{p}^{\mathrm{L}}_{i,s,t}$ depending on the value of $\sigma_{s,t}$. Based on this observation, (23) can be derived from (14d) and (14m). For energy storage, (24) can be further derived from (21).

$$\tilde{p}^{\mathrm{U}}_{i,s,t} \le p_{i,s,t} \le \tilde{p}^{\mathrm{L}}_{i,s,t} \quad \forall i \in \Omega_{\mathrm{g}} \cup \Omega_{\mathrm{ng}} \cup \Omega_{\mathrm{nes}}, s, t \tag{23}$$

$$\tilde{p}^{\mathrm{dc\ U}}_{i,s,t} \le p^{\mathrm{dc}}_{i,s,t} \le \tilde{p}^{\mathrm{dc\ L}}_{i,s,t}, \quad \tilde{p}^{\mathrm{ch\ L}}_{i,s,t} \le p^{\mathrm{ch}}_{i,s,t} \le \tilde{p}^{\mathrm{ch\ U}}_{i,s,t} \quad \forall i \in \Omega_{\mathrm{nes}}, s, t \tag{24}$$

The ramp constraints in (5b) and (5d) are satisfied for any $wc \in U'$ under the given solution, as shown in (25). The inequalities (a) and (d) are ensured by (14g)-(14h), while (b) and (c) can be obtained from (23).

$$\begin{aligned} -RD_i \cdot \hat{n}_i &\overset{(a)}{\le} \tilde{p}^{\mathrm{U}}_{i,s,t+1} - \tilde{p}^{\mathrm{L}}_{i,s,t} \overset{(b)}{\le} p_{i,s,t+1} - p_{i,s,t} \\ &\overset{(c)}{\le} \tilde{p}^{\mathrm{L}}_{i,s,t+1} - \tilde{p}^{\mathrm{U}}_{i,s,t} \overset{(d)}{\le} RU_i \cdot \hat{n}_i \end{aligned} \tag{25}$$

For the SOC bounds of storage, in (26), (e) and (h) are established from (14n)-(14q) as shown previously in (10). With coefficients $\delta_i, \eta^{\mathrm{ch}}_i, \eta^{\mathrm{dc}}_i \in (0,1)$, (f) and (g) can be obtained from (24). Thus, for any $wc \in U'$, constraints (6e)-(6h) is satisfied under the given solution.

$$\begin{aligned} &\underline{\gamma}_{i,s,t} E_i - (1-\delta_i)^t \gamma_{i,s,0} E_i \\ &\overset{(e)}{\le} \sum_{t'=1}^{t} (1-\delta_i)^{t-t'} \left(\eta^{\mathrm{ch}}_i \cdot \tilde{p}^{\mathrm{ch\ L}}_{i,s,t'} - 1/\eta^{\mathrm{dc}}_i \cdot \tilde{p}^{\mathrm{dc\ L}}_{i,s,t'}\right) \\ &\overset{(f)}{\le} \sum_{t'=1}^{t} (1-\delta_i)^{t-t'} \left(\eta^{\mathrm{ch}}_i \cdot p^{\mathrm{ch}}_{i,s,t'} - 1/\eta^{\mathrm{dc}}_i \cdot p^{\mathrm{dc}}_{i,s,t'}\right) \\ &\overset{(g)}{\le} \sum_{t'=1}^{t} (1-\delta_i)^{t-t'} \left(\eta^{\mathrm{ch}}_i \cdot \tilde{p}^{\mathrm{ch\ U}}_{i,s,t'} - 1/\eta^{\mathrm{dc}}_i \cdot \tilde{p}^{\mathrm{dc\ U}}_{i,s,t'}\right) \\ &\overset{(h)}{\le} \overline{\gamma}_{i,s,t} E_i - (1-\delta_i)^t \gamma_{i,s,0} E_i \end{aligned} \tag{26}$$

Thus, we conclude there exists a feasible solution for constraints (4)-(6) with any $wc \in U'$ if (14) is feasible.

2) Proof for U: Our conclusion is then extended from U' to U. As shown in (27), the terms related to the net load in (4) is defined by $r_{s,t}$.

$$r_{s,t} = d_{s,t} - \sum\nolimits_{i \in \Omega_{\mathrm{w}}} wc_{i,s,t} \cdot \hat{P}_i - \sum\nolimits_{i \in \Omega_{\mathrm{nw}}} wc_{i,s,t} \cdot P_i \tag{27}$$

For $wc \in U'$, a set formed by corresponding vector r (we define $r = \{r_{s,t},\ \forall s,t\}$) is denoted as V'. The set of V' can also be represented by enumerating all the values of $\sigma_{s,t}$ in (16), as shown in (28).

$$\begin{aligned} V' = &\\ &\left\{ \begin{array}{l} r \in \mathbb{R}^{N_s \cdot N_t} : r_{s,t} = d_{s,t} - \sum_{i \in \Omega_{\mathrm{w}}} wc^{\mathrm{L}}_{i,s,t} \cdot \hat{P}_i - \\ \sum_{i \in \Omega_{\mathrm{nw}}} wc^{\mathrm{L}}_{i,s,t} \cdot P_i - \sigma_{s,t} \cdot \Big[\sum_{i \in \Omega_{\mathrm{w}}} \left(wc^{\mathrm{U}}_{i,s,t} - wc^{\mathrm{L}}_{i,s,t}\right) \cdot \\ \hat{P}_i + \sum_{i \in \Omega_{\mathrm{nw}}} \left(wc^{\mathrm{U}}_{i,s,t} - wc^{\mathrm{L}}_{i,s,t}\right) \cdot P_i \Big],\ \sigma_{s,t} \in \mathbb{B},\ \forall s,t \end{array} \right\} \\ &= \{v_1, v_2, ..., v_{2^{N_s \cdot N_t}}\} \end{aligned} \tag{28}$$

Analogously, for any $wc \in U$, the corresponding r forms a set of V. As a matter of fact, V extends the binary variable $\sigma_{s,t}$ in V' to a range of $[0,1]$. It can be represented by a convex combination form based on vertices of V', as shown in (29). In this case, V is the convex hull of V'.

$$V = \Big\{ w \in \mathbb{R}^{N_s \cdot N_t} : w = \textstyle\sum_{k=1}^{2^{N_s \cdot N_t}} \alpha_k v_k, \ \sum_{k=1}^{2^{N_s \cdot N_t}} \alpha_k = 1,\ \alpha_k \ge 0 \Big\} \tag{29}$$

For any $wc \in U$ (i.e., $w \in V$), a feasible solution of constraints (4)-(6) can be represented in (30)-(32), wherein $p^{(k)}_{i,s,t}$ represents a solution of injection power in the k-th combination of $\sigma_{s,t}$.

$$p_{i,s,t} = \sum\nolimits_{k=1}^{2^{N_s \cdot N_t}} \alpha_k p^{(k)}_{i,s,t} \quad \forall i \in \Omega_{\mathrm{g}} \cup \Omega_{\mathrm{ng}} \cup \Omega_{\mathrm{nes}}, s, t \tag{30}$$

$$p^{\mathrm{dc}}_{i,s,t} = \max\left\{p_{i,s,t}, 0\right\}, \quad p^{\mathrm{ch}}_{i,s,t} = -\min\left\{p_{i,s,t}, 0\right\} \quad \forall i \in \Omega_{\mathrm{nes}}, s, t \tag{31}$$

$$u^{\mathrm{dc}}_{i,s,t} = \max\left\{\mathrm{sgn}\left(p_{i,s,t}\right), 0\right\}, \quad u^{\mathrm{ch}}_{i,s,t} = 1 - u^{\mathrm{dc}}_{i,s,t} \quad \forall i \in \Omega_{\mathrm{nes}}, s, t \tag{32}$$

The non-temporal constraints (4), (5a), (5c), and (6a)-(6d) can also be trivially verified. With the convex combination property in (29) and (30), equations (23) and (24) still hold. In a similar manner to the previous proof, ramp constraints (5b), (5d), and SOC constraints (10) can also be verified. ∎

The property shown in this subsection ensures that any investment decision satisfying constraints (14) can cover all the cases in the uncertainty set in (15). Meanwhile, our approach is iteration-free, and the number of constraints keeps on a moderate size to avoid the curse of dimensionality.

C. Bi-Interval Policy

To reduce the conservativeness of the planning problem, a bi-interval policy is further proposed in this subsection.

1) Framework Description: If load shedding and renewable power curtailment are not allowed, the resultant investment decision that can address all possible cases might be expensive, as a large portion of the high investment cost might be paid for rarely happened cases. To tackle this, we define an inner interval based uncertainty set for cases that commonly happen, while all the possible cases including those rarely happen are incorporated in an outer interval based uncertainty set. Distinct operation rules are applied for these two sets. For convenience, IO constraints for the inner set $[wc^{\mathrm{L}}, wc^{\mathrm{U}}]$ are presented in (14). We define the outer set as $[wc^{\mathrm{EL}}, wc^{\mathrm{EU}}]$. The corresponding IO constraints are shown later in (33).

Different load shedding and renewable power curtailment policies are applied for the two sets:

a. For the inner interval based uncertainty set, as only normal scenarios are incorporated, load shedding is not allowed to achieve a reliable power supply, and renewable energy curtailment is also not encouraged according to Article 14 of *Renewable Energy Law* of China [20].

b. For extreme cases in the outer interval based uncertainty set, the system security is the most critical concern. Load

shedding is subject to *Regulations on Emergency Handling, Investigation and Disposal of Electric Power Safety Accidents* in China [21], which restricts shedding proportions for various types of power systems. Renewable energy curtailment is also considered an emergency control measure for such cases.

The bi-interval policy has the advantage of guaranteeing system power balance in any possible cases, and preventing load shedding and renewable power curtailment in most common cases. This design aims to avoid paying a high price for rarely happened cases, therefore a better trade-off between system security and investment cost could be achieved.

2) IO Constraints for the Outer Interval Based Uncertainty Set: After taking load shedding and renewable power curtailment limits into consideration, the constraints for the outer interval based uncertainty set are presented in (33). In fact, the key differences lie in the system balance constraints in (33a), renewable power curtailment limits in (33b), and load shedding limits in (33c). Similarly, it can also be proved investment decisions that satisfy constraints (33) can cover all the cases in the given outer interval based uncertainty set.

$$\sum\nolimits_{i\in\Omega_{\mathrm{g}}\cup\Omega_{\mathrm{ng}}} p_{i,s,t}^{\mathrm{EU(EL)}} + \sum\nolimits_{i\in\Omega_{\mathrm{nes}}} p_{i,s,t}^{\mathrm{EU(EL)}} = d_{s,t} - d_{s,t}^{\mathrm{s\ EU(EL)}} - \left(\sum\nolimits_{i\in\Omega_{\mathrm{w}}} wc_{i,s,t}^{\mathrm{EU(EL)}} \cdot \hat{P}_i + \sum\nolimits_{i\in\Omega_{\mathrm{nw}}} wc_{i,s,t}^{\mathrm{EU(EL)}} \cdot P_i - w_{s,t}^{\mathrm{c\ EU(EL)}} \right) \quad \forall s,t \tag{33a}$$

$$0 \le w_{s,t}^{\mathrm{c\ EU(EL)}} \le \sum\nolimits_{i\in\Omega_{\mathrm{w}}} wc_{i,s,t}^{\mathrm{EU(EL)}} \cdot \hat{P}_i + \sum\nolimits_{i\in\Omega_{\mathrm{nw}}} wc_{i,s,t}^{\mathrm{EU(EL)}} \cdot P_i \quad \forall s,t \tag{33b}$$

$$0 \le d_{s,t}^{\mathrm{s\ EU(EL)}} \le \varphi \cdot d_{s,t} \quad \forall s,t \tag{33c}$$

Eq. (14b)-(14q) with subscripts U(L) replaced by EU(EL) (33d)

Finally, the overall problem is formulated in a non-iterative mixed-integer linear program (MILP) with objective function (1) and constraints (2)-(7). The detailed formulation for (7) is expressed in constraints (14) and (33).

V. Case Study

A modified IEEE 24-bus reliability test system (RTS) and a real-world Gansu provincial power grid in China are used to test the proposed approach. The MILP problems in this paper were solved by Cplex 12.8 [22] on a computer with dual Intel Xeon CPU E5-2650 and 128GB RAM.

A. Modified IEEE 24-Bus Reliability Test System: Verification of the Proposed Approach

The IEEE RTS [23] contains 32 generators with 3405 MW of total installed capacity. For planning purposes, the demands are assumed as 2 times their original values. Wind and photovoltaic (PV) power stations are also included as investment candidates. The data for existing and candidate generators is from [23], [24]. The results of generation expansion planning are shown in Fig. 2 under different carbon emission targets. As indicated, the capacity and share of renewable energy sources

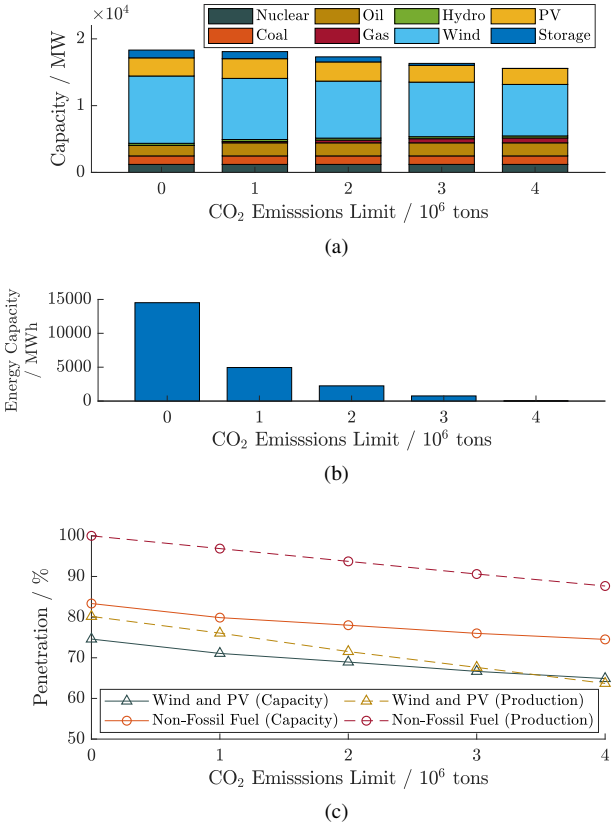

Fig. 2. Planning results for IEEE RTS: (a) generation mix, (b) energy capacity of storage, (c) share of non-hydro renewable energy sources and non-fossil fuel energy sources.

generally increase as the emission limit decreases. This leads to stronger requirements for energy storage on shaving the peak load and storing surplus renewable energy. Therefore, larger storage capacities are shown in the GEP decisions with lower carbon-emission limits. Our method to choose an inner interval based uncertainty set for this case is provided in supplementary material [25].

1) Numerical Error Analysis for the CSM: In this work, the CSM is implemented in (8) and (6d)-(6h). Comparisons of storage investment decisions from both DSM and CSM are shown in Table II. As indicated, the CSM results in a considerable amount of error in both power and energy capacities for energy storage, especially when the penetration of renewable energy is high. We observe the energy capacity

TABLE II
Error Analysis for CSM in IEEE RTS

CO_2 emission limit (10^6 tons)		0	1	2	3	4
power capacity (MW)	DSM	1163.6 (46.3%)	1058.4 (91.9%)	757.5 (100.0%)	285.2 (88.6%)	16.5 (100.0%)
	CSM	2514.1 (100.0%)	1151.8 (100.0%)	709.9 (93.7%)	322.0 (100.0%)	7.7 (46.5%)
energy capacity (MWh)	DSM	14518.9 (100.0%)	4951.6 (100.0%)	2245.0 (100.0%)	758.5 (100.0%)	15.2 (100.0%)
	CSM	8516.3 (58.7%)	3888.9 (78.5%)	1891.4 (84.2%)	550.7 (72.6%)	7.1 (46.5%)

TABLE III
INVESTMENT COST COMPARISON OF SP, RO AND IO IN IEEE RTS

method	# of scenarios considered in SP	investment cost (10^9\$)			
		conventional generators	renewable energy stations	energy storage	total
SP	1	1.69	24.56	0.95	27.19
	10	1.69	23.99	2.30	27.99
	20	1.69	23.98	2.52	28.20
	30	1.69	23.98	2.52	28.20
RO	-	2.18	24.13	143.44	169.75
IO (w/o BIP)	-	2.18	24.13	143.44	169.75
IO (w/ BIP)	-	2.89	23.67	4.50	31.06

TABLE IV
MCS-BASED COMPARISON OF SP, RO, AND IO SOLUTIONS IN IEEE RTS

method	# of scenarios considered in SP	# of MCS samples with renewable curtailment or load shedding	expected operation cost for feasible samples (10^7\$)
SP	1	905 (90.5%)	4.45 (5 samples)
	10	109 (10.9%)	4.54 (891 samples)
	20	46 (4.6%)	4.54 (954 samples)
	30	46 (4.6%)	4.54 (954 samples)
RO	-	0 (0%)	5.00 (1000 samples)
IO (w/o BIP)	-	0 (0%)	5.00 (1000 samples)
IO (w/ BIP)	-	1 (0.1%)	4.75 (999 samples)

from CSM is less than that from DSM, which would reduce the investment cost term $\beta_i \cdot E_i$ in the CSM cases. Fig. 1 in section III shows simultaneous charging and discharging behavior exists when using the CSM in GEP. The simulation results in Table II also match with our analysis in section III.

2) Comparison to Robust and Stochastic Approaches: The proposed IO approach is compared to SP and RO with DSM in the operation stage. Monte Carlo simulations (MCS) with 1000 samples are performed to evaluate operating performance under given investment decisions. For this test system, wind and PV generation levels are assumed to follow Weibull [26] and Beta [27] distributions, respectively.

Table III shows the investment cost for IEEE RTS from different approaches under 2×10^6 tons CO_2 emission limit. The after-fact evaluation of system security and expected operation cost is presented in Table IV. As indicated in Table IV, in comparison to the proposed approach, the investment decision from SP leads to more MCS samples with renewable curtailment or load shedding, which is considered less secure. Although the security level can be improved with more scenarios included in SP, it would be computational intractable to incorporate all scenarios. RO and IO based approaches are both secure as indicated in Table IV. However, as shown in Table III, they are more expensive in terms of investment cost. Our proposed IO together with bi-interval policy (denoted as "w/ BIP" in Tables III and IV) can reduce the overall cost, meanwhile maintaining a high system security level.

In addition, we can observe that the IO without bi-interval policy (denoted as "w/o BIP" in Tables III and IV) performs almost the same with RO in both cost and security level. Although the IO (without bi-interval policy) formulation is theoretically tighter than RO as analyzed in section IV, its practical performance almost matches that of RO in conservativeness. In addition, RO with DSM in the operation stage usually needs to be implemented in a nested iterative approach [11], while our proposed approach is iteration-free.

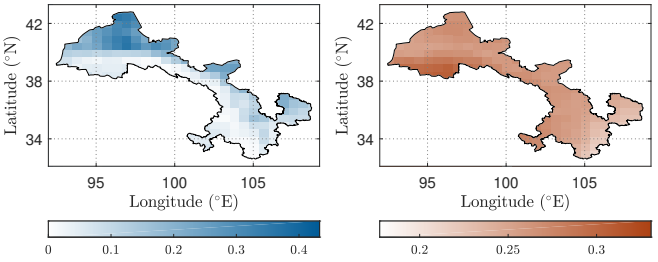

Fig. 3. Geographical distributions of maximum capacity factors for wind and PV systems: (a) wind, (b) PV.

B. Gansu Power Grid: Prospects of Energy Storage

1) Data Settings: Located in northwest China, Gansu province has abundant wind and solar resources. The resource potentials and normalized available generation curves for renewable energy sources are estimated based on the methods in [28]–[31]. In detail, the digital elevation model (DEM) and land use data are from [32], [33], and the meteorological data for wind and solar resources are from ERA5 [34] and MERRA-2 [35], respectively. The geographical distributions of maximum capacity factors for wind and PV systems are shown in Fig. 3. Sites with high maximum capacity factors are selected as candidates. Candidate generators for this planning problem include coal-fired and gas-fired generators. Economic resources for conventional hydro generators have almost been fully developed, so conventional hydro generators are not considered candidates. The technological types for energy storage candidates are pumped storage and carbon-lead (PbC) battery storage. The details of choosing an inner interval based uncertainty set for this case are also provided in [25].

2) Summary of Method Verification: Error analysis on battery storage sizing for using the CSM in GEP is conducted for the Gansu system. As shown in Table V, the comparison again verifies that the CSM usually results in significant errors in energy capacity investment decisions for storage. The energy capacity from the CSM is also less than that from the DSM.

TABLE V
ERROR ANALYSIS FOR CSM IN GANSU POWER GRID

CO_2 emission limit (10^7 tons)		0	3	6	9
power capacity (MW)	DSM	48014.7 (25.8%)	22614.7 (59.9%)	8675.2 (100.0%)	550.2 (100.0%)
	CSM	186406.8 (100.0%)	37736.5 (100.0%)	8397.6 (96.8%)	550.1 (100.0%)
energy capacity (MWh)	DSM	548718.7 (100.0%)	103954.0 (100.0%)	30987.4 (100.0%)	504.3 (100.0%)
	CSM	191628.9 (34.9%)	74943.0 (72.1%)	28659.4 (92.5%)	504.1 (100.0%)

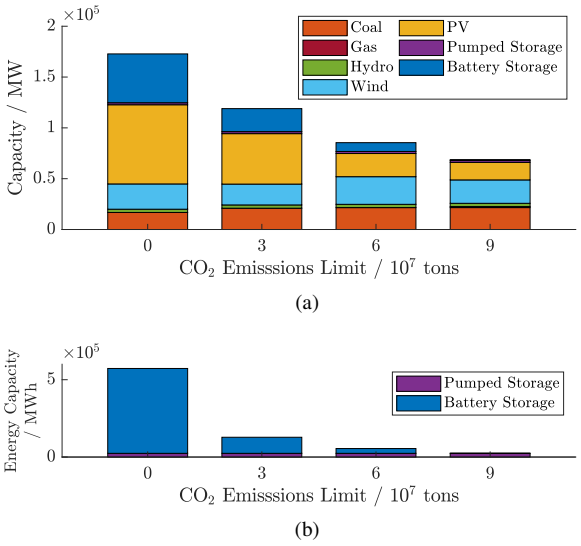

Fig. 4. Planning results for Gansu power grid: (a) generation mix, (b) energy capacity of energy storage.

Leveraging negative $\eta_i^{\text{ch}} - 1/\eta_i^{\text{dc}}$ value in (11), the investment cost term $\beta_i \cdot E_i$ is reduced in the CSM case. Note although the storage capacity difference is not large in the case of 9×10^7 tons emission limit, the energy capacity from the CSM is still smaller. The numerical results also match with our analysis in section III. To evaluate the security performance of the proposed IO (with bi-interval policy) approach, Monte Carlo simulations are also conducted. As a result, all the 1000 generated cases pass the operational feasibility test.

3) The Role of Energy Storage: The generation mix and storage capacity are shown in Fig. 4 under different emission targets. The capacity of renewable energy sources increases with the decrease of CO_2 emission limit, making the fluctuations of the power supply more significant. This leads to stronger requirements for energy storage on shaving the peak load and storing surplus renewable energy, thus larger storage capacities are shown in the GEP decisions. The GEPs are also solved without energy storage candidates for comparisons, which comes out with infeasibilities of the optimization problems for listed cases with emission limits less than 9×10^7 tons. This indicates energy storage is an essential option for a low-carbon power system.

Given the price for battery storage is expected to decrease in the future, a sensitivity analysis is performed to assess the impact of storage investment cost on the generation mix and the overall cost. Taking the case of zero carbon emission in the operation phase as an example, the cost per unit of power capacity α and the cost per unit of energy capacity β are the coefficients used to analyze. As indicated by the results of sensitivity analysis in Fig. 5, the overall cost decreases as both the cost per unit of power capacity α and the cost per unit of energy capacity β decrease. However, as shown in Fig. 5e, β has a more significant impact on the generation mix, the storage capacity, and the overall cost. Thus, reducing the cost per unit of energy capacity for battery storage is a critical factor to realize a high renewable energy penetrated system.

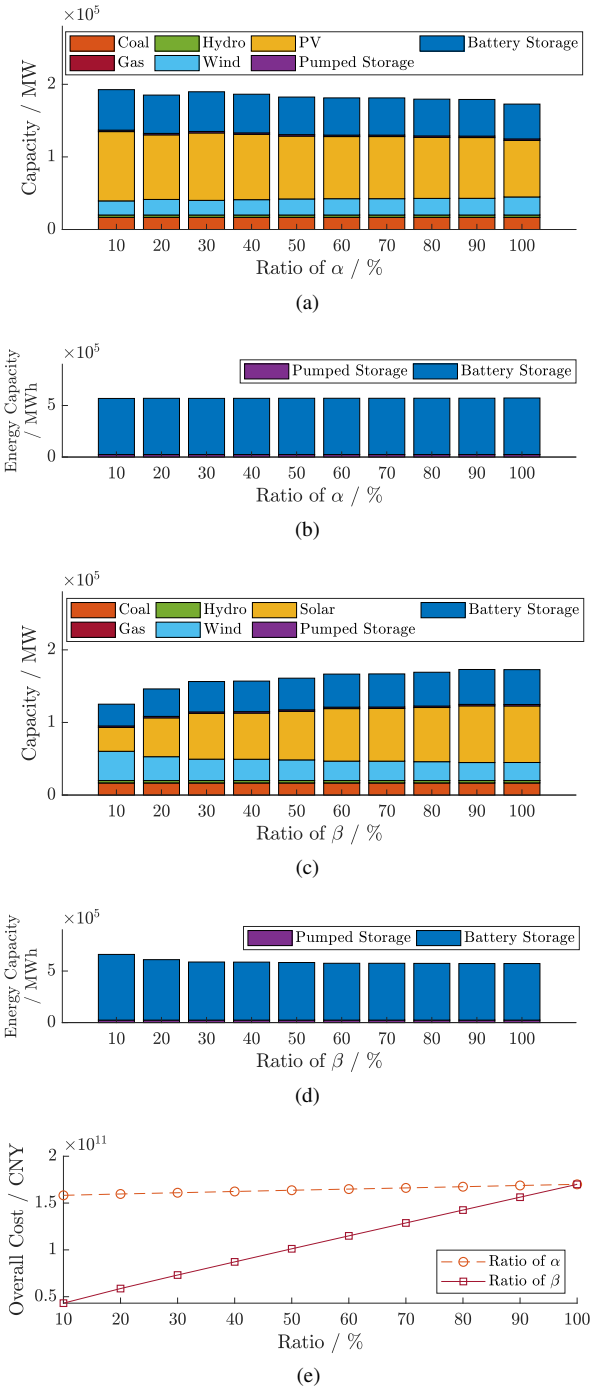

Fig. 5. Sensitivity analysis for coefficients of energy storage: (a) generation mix under different α, (b) energy capacity of storage under different α, (c) generation mix under different β, (d) energy capacity of storage under different β, (e) the overall cost under different α and β.

VI. Conclusion

This paper proposes a bi-interval policy embedded IO approach for GEP with DSM in the operation stage. The main findings in this work are,

1) The CSM could result in simultaneous charging and discharging, which could benefit the energy capacity related term of investment cost in GEP, due to the inherent energy conversion losses modeled in the SOC constraints.

2) Given the DSM is incorporated in the operation stage, the proposed IO approach can cover all the cases in a pre-specified uncertainty set. Numerical results show IO (without bi-interval policy) performs almost the same as RO in conservativeness. In comparison to SO and RO, the proposed IO together with bi-interval policy can effectively reduce the investment cost, while maintaining a high system security level.

3) Energy storage is shown to be an essential option for a low carbon future in Gansu power grid. The investment cost per unit of energy capacity of battery storage has a significant impact on the overall system cost.

For future works, the proposed approach can be extended to incorporate LP approximated unit commitment constraints. In addition, as only the short-term system operation security is guaranteed under renewable energy uncertainty in this work, the effect of uncertainty on the long-term carbon emission target can be further investigated.

ACKNOWLEDGMENT

The authors would like to thank Yan Chen for the helpful discussion on geographic data processing approaches.

REFERENCES

[1] S. Wang, "Energy storage planning for large scale renewable energy integrated power systems," Ph.D. dissertation, Zhejiang Univ., Hangzhou, China, 2019, in Chinese.

[2] W. Lyzwa, M. Wierzbowski, and B. Olek, "MILP formulation for energy mix optimization," *IEEE Trans. on Industr. Inform.*, vol. 11, no. 5, pp. 1166–1178, 2015.

[3] O. M. Babatunde, J. L. Munda, and Y. Hamam, "A comprehensive state-of-the-art survey on power generation expansion planning with intermittent renewable energy source and energy storage," *Int. J. Energy Res.*, vol. 43, no. 12, pp. 6078–6107, 2019.

[4] M. Alhaider and L. Fan, "Planning energy storage and photovoltaic panels for demand response with heating ventilation and air conditioning systems," *IEEE Trans. on Industr. Inform.*, vol. 14, no. 11, pp. 5029–5037, 2018.

[5] P. Yang and A. Nehorai, "Joint optimization of hybrid energy storage and generation capacity with renewable energy," *IEEE Trans. Smart Grid*, vol. 5, no. 4, pp. 1566–1574, 2014.

[6] T. Qiu, B. Xu, Y. Wang, Y. Dvorkin, and D. S. Kirschen, "Stochastic multistage coplanning of transmission expansion and energy storage," *IEEE Trans. on Power Syst.*, vol. 32, no. 1, pp. 643–651, 2016.

[7] X. Zhang and A. J. Conejo, "Coordinated investment in transmission and storage systems representing long-and short-term uncertainty," *IEEE Trans. on Power Syst.*, vol. 33, no. 6, pp. 7143–7151, 2018.

[8] H. Alharbi and K. Bhattacharya, "Stochastic optimal planning of battery energy storage systems for isolated microgrids," *IEEE Trans. Sustain. Energy*, vol. 9, no. 1, pp. 211–227, 2017.

[9] R. A. Jabr, I. Džafić, and B. C. Pal, "Robust optimization of storage investment on transmission networks," *IEEE Trans. on Power Syst.*, vol. 30, no. 1, pp. 531–539, 2014.

[10] S. Dehghan and N. Amjady, "Robust transmission and energy storage expansion planning in wind farm-integrated power systems considering transmission switching," *IEEE Trans. Sustain. Energy*, vol. 7, no. 2, pp. 765–774, 2015.

[11] S. Wang, G. Geng, and Q. Jiang, "Robust co-planning of energy storage and transmission line with mixed integer recourse," *IEEE Trans. on Power Syst.*, vol. 34, no. 6, pp. 4728–4738, 2019.

[12] Z. Li, Q. Guo, H. Sun, and J. Wang, "Sufficient conditions for exact relaxation of complementarity constraints for storage-concerned economic dispatch," *IEEE Trans. Power Syst.*, vol. 31, no. 2, pp. 1653–1654, 2015.

[13] J. M. Arroyo, L. Baringo, A. Baringo, R. Bolaños, N. Alguacil, and N. G. Cobos, "On the use of a convex model for bulk storage in MIP-based power system operation and planning," *IEEE Trans. on Power Syst.*, vol. 35, no. 6, pp. 4964–4967, 2020.

[14] J. Chinneck and K. Ramadan, "Linear programming with interval coefficients," *J. Oper. Res. Soc.*, vol. 51, no. 2, pp. 209–220, 2000.

[15] Y. Wang, Q. Xia, and C. Kang, "Unit commitment with volatile node injections by using interval optimization," *IEEE Trans. Power Syst.*, vol. 26, no. 3, pp. 1705–1713, 2011.

[16] B. Zhou, G. Geng, and Q. Jiang, "Hierarchical unit commitment with uncertain wind power generation," *IEEE Trans. Power Syst.*, vol. 31, no. 1, pp. 94–104, 2015.

[17] Z. Wang, C. Song, L. Zhang, Y. Zhao, P. Liu, and D. G. Dorrell, "A data-driven method for battery charging capacity abnormality diagnosis in electric vehicle applications," *IEEE Trans. Transp. Electrification*, 2021.

[18] X. Hu, H. Yuan, C. Zou, Z. Li, and L. Zhang, "Co-estimation of state of charge and state of health for lithium-ion batteries based on fractional-order calculus," *IEEE Trans. Veh. Technol.*, vol. 67, no. 11, pp. 10 319–10 329, 2018.

[19] C. She, L. Zhang, Z. Wang, F. Sun, P. Liu, and C. Song, "Battery state of health estimation based on incremental capacity analysis method: synthesizing from cell-level test to real-world application," *IEEE Trans. Emerg. Sel. Topics Power Electron.*, 2021.

[20] Renewable energy law of China. [Online]. Available: http://english.gov.cn/archive/laws_regulations/2014/08/23/con\tent_281474983043598.htm

[21] State Council of the China. Order No. 599, regulations on emergency handling, investigation and disposal of electric power safety accidents. [Online]. Available: http://www.gov.cn/flfg/2011-07/15/content_1908466.htm

[22] IBM. ILOG CPLEX Homepage. Armonk, NY, USA. [Online]. Available: http://www.ilog.com

[23] C. Grigg *et al.*, "The IEEE reliability test system-1996. a report prepared by the reliability test system task force of the application of probability methods subcommittee," *IEEE Trans. Power Syst.*, vol. 14, no. 3, pp. 1010–1020, 1999.

[24] S. Dehghan, N. Amjady, and A. Kazemi, "Two-stage robust generation expansion planning: a mixed integer linear programming model," *IEEE Trans. Power Syst.*, vol. 29, no. 2, pp. 584–597, 2013.

[25] S. Wang, G. Geng, Q. Jiang, and R. Bo. Supplementary material for "generation expansion planning considering discrete storage model and renewable energy uncertainty: A bi-interval optimization approach". [Online]. Available: https://github.com/ee-swang/supplementary-material/blob/main/SUPPL-TII-22-0321.pdf

[26] A. Altunkaynak, T. Erdik, İ. Dabanlı, and Z. Şen, "Theoretical derivation of wind power probability distribution function and applications," *Appl. Energy*, vol. 92, pp. 809–814, 2012.

[27] V. Graham and K. Hollands, "A method to generate synthetic hourly solar radiation globally," *Sol. Energy*, vol. 44, no. 6, pp. 333–341, 1990.

[28] G. He and D. M. Kammen, "Where, when and how much wind is available? a provincial-scale wind resource assessment for China," *Energy Policy*, vol. 74, pp. 116–122, 2014.

[29] G. He and D. M. Kammen, "Where, when and how much solar is available? a provincial-scale solar resource assessment for China," *Renew. Energy*, vol. 85, pp. 74–82, 2016.

[30] T. Huld, R. Gottschalg, H. G. Beyer, and M. Topič, "Mapping the performance of PV modules, effects of module type and data averaging," *Sol. Energy*, vol. 84, no. 2, pp. 324–338, 2010.

[31] S. Pfenninger and I. Staffell, "Long-term patterns of European PV output using 30 years of validated hourly reanalysis and satellite data," *Energy*, vol. 114, pp. 1251–1265, 2016.

[32] Chinese Academy of Sciences. Cold and arid regions sciences data center at Lanzhou. Lanzhou, China. [Online]. Available: http://westdc.westgis.ac.cn

[33] J. Liu, M. Liu, D. Zhuang, Z. Zhang, and X. Deng, "Study on spatial pattern of land-use change in China during 1995–2000," *Sci. China Earth Sci.*, vol. 46, no. 4, pp. 373–384, 2003.

[34] European Centre for Medium-Range Weather Forecasts. ERA5 data documentation. Reading, UK. [Online]. Available: https://confluence.ecmwf.int/display/CKB/ERA5+data+documentation

[35] R. Gelaro *et al.*, "The modern-era retrospective analysis for research and applications, version 2 (MERRA-2)," *J. Clim.*, vol. 30, no. 14, pp. 5419–5454, 2017.

Siyuan Wang received the B.S. and Ph.D. degrees in electrical engineering from Zhejiang University, Hangzhou, China, in 2013 and 2019, respectively. He is currently a Postdoctoral Fellow with the Whiting School of Engineering, Johns Hopkins University, Baltimore, MD, USA. From 2019 to 2022, he was a Postdoctoral Fellow with the Department of Electrical and Computer Engineering, Missouri University of Science and Technology (formerly University of Missouri-Rolla), Rolla, MO, USA. His research interests include power system operation and planning, renewable energy integration, and applications of energy storage technology in power systems.

Guangchao Geng (Senior Member, IEEE) received the B.S. and Ph.D. degrees in electrical engineering from the College of Electrical Engineering, Zhejiang University, Hangzhou, China, in 2009 and 2014, respectively. He is currently an Associate Professor with the College of Electrical Engineering, Zhejiang University, Hangzhou, China. From 2012 to 2013, he was a Visiting Student with the Department of Electrical and Computer Engineering, Iowa State University, Ames, IA, USA. From 2014 to 2017, he was a Postdoctoral Fellow with the College of Control Science and Engineering, Zhejiang University, Hangzhou, China, and the Department of Electrical and Computer Engineering, University of Alberta, Edmonton, AB, Canada. His research interests include power system stability and control, renewable energy integration, and high performance computing.

Quanyuan Jiang (Senior Member, IEEE) received the B.S., M.S., and Ph.D. degrees in electrical engineering from the Huazhong University of Science and Technology, Wuhan, China, in 1997, 2000, and 2003, respectively. He is currently a Professor with the College of Electrical Engineering, Zhejiang University, Hangzhou, China. From 2006 to 2008, he was a Visiting Associate Professor with the School of Electrical and Computer Engineering, Cornell University, Ithaca, NY, USA. His research interests include power system stability and control, high performance computing, and applications of energy storage systems in power systems.

Rui Bo (Senior Member, IEEE) received the BSEE and MSEE degrees in electric power engineering from Southeast University (China) in 2000 and 2003, respectively, and received the Ph.D. degree in electrical engineering from the University of Tennessee, Knoxville (UTK) in 2009. He is currently an Assistant Professor of the Electrical and Computer Engineering Department with the Missouri University of Science and Technology (formerly University of Missouri-Rolla). He worked as a Principal Engineer and Project Manager at Midcontinent Independent System Operator (MISO) from 2009 to 2017. His research interests include computation, optimization and economics in power system operation and planning, high performance computing, electricity market simulation, evaluation and design.